Article

Insights into the Structural Determinants Required for High Affinity Binding of Chiral Cyclopropane-Containing Ligands to #4#2-Nicotinic Acetylcholine Receptors; An Integrated Approach to Behaviorally Active Nicotinic Ligands

Han-Kun Zhang, J. Brek Eaton, Li-Fang Yu, Mieke Nys, Angelica Mazzolari, René van Elk, August B. Smit, Vadim Alexandrov, Taleen Hanania, Emily Sabath, Allison Fedolak, Daniela Brunner, Ronald J. Lukas, Giulio Vistoli, Chris Ulens, and Alan P. Kozikowski

J. Med. Chem., **Just Accepted Manuscript** • DOI: 10.1021/jm3008739 • Publication Date (Web): 28 Aug 2012

Insights into the Structural Determinants Required for High Affinity Binding of Chiral Cyclopropane-Containing Ligands to α4β2-Nicotinic Acetylcholine Receptors; An Integrated Approach to Behaviorally Active Nicotinic Ligands

Han-Kun Zhang,[†] J. Brek Eaton,[‡] Li-Fang Yu,[†] Mieke Nys,[§] Angelica Mazzolari,[⊥] René van Elk,[‖] August B. Smit,[‖] Vadim Alexandrov,[Δ] Taleen Hanania,[Δ] Emily Sabath,[Δ] Allison Fedolak,[Δ] Daniela Brunner,*[,Δ,#] Ronald J. Lukas,*[,‡] Giulio Vistoli,*[,⊥] Chris Ulens,*[,§] and Alan P. Kozikowski*[,†]

[†]Drug Discovery Program, Department of Medicinal Chemistry and Pharmacognosy, University of Illinois at Chicago, 833 South Wood Street, Chicago, Illinois 60612, [‡]Division of Neurobiology, Barrow Neurological Institute, 350 West Thomas Road, Phoenix, Arizona 85013, [§]Laboratory of Structural Neurobiology, Dept. of Cellular and Molecular Medicine, Herestraat 49, PB 601, B-3000 Leuven, Belgium, [⊥]Dipartimento di Scienze Farmaceutiche "Pietro Pratesi", Università degli Studi di Milano, Via Mangiagalli 25, I-20133, Milan, Italy, [‖]Department of Molecular & Cellular Neurobiology, Center for Neurogenomics and Cognitive Research, Neuroscience Campus Amsterdam, VU University, The Netherlands, [Δ]PsychoGenics, Inc., 765 Old Saw Mill River Road, Tarrytown, New York 10591, and [#]Department of Psychiatry, Columbia University, NYSPI, 1051 Riverside Drive, New York 10032.

ABSTRACT: Structure-based drug design can potentially accelerate the development of new therapeutics. In this study, a co-crystal structure of the acetylcholine binding protein (AChBP) from *Capitella teleta* (Ct) in complex with a cyclopropane-containing, selective α4β2-nicotinic acetylcholine receptor (nAChR) partial agonist (compound **5**) was acquired. The structural determinants required for ligand binding obtained from this AChBP X-ray structure were used to refine our previous model of the human α4β2-nAChR, thus possibly providing a better understanding of the structure of the human receptor. In order to validate the potential application of the structure of the Ct-AChBP in the engineering of new α4β2-nAChR ligands, homology modeling methods, combined with *in silico* ADME calculations, were used to design analogs of compound **5**. The most promising compound **12**, exhibited an improved metabolic stability in comparison to the parent compound **5** while retaining favorable pharmacological parameters together with appropriate behavioral endpoints in the rodent studies.

Introduction

Nicotinic acetylcholine receptors (nAChRs) belong to the Cys-loop superfamily of ligand-gated ion channels (LGICs) that also include 5-HT_3, $GABA_{A/C}$, and glycine receptors.[1] They are widely distributed in the central and peripheral nervous systems, where they broadly participate in regulating major physiological functions and pathophysiological processes associated with learning and memory, mood, reward, motor control, arousal, analgesia, and inflammation.[2, 3] Mammalian neuronal nAChRs are homo- or heteromeric pentamers assembled from diverse combinations of subunits (α2–α10 and β2–β4). The variety in subtype stoichiometries results in neuronal nAChRs that exhibit highly variable properties in regard to ligand pharmacology, activation and desensitization kinetics, cation permeability, and subcellular and regional distribution. Each nAChR subunit consists of a large amino-terminal extracellular domain (ECD), a transmembrane domain comprising four α-helices (M1–M4), and a variable cytoplasmic domain between M3 and M4. Acetylcholine (ACh) binding sites are thought to be formed between the subunit interfaces of the ECD that involve so-called loops A–C on the principle face

of an α-type subunit and the adjacent, complementary face of the neighboring subunit involving loops D–F. Known heteromeric pentamers have a minimum of two α-type subunits whereas homopentamers have five, resulting in two to five ACh-binding sites within the ECD, the occupancy of which by ACh or other agonists leads to global allosteric transitions of the receptor protein that mediate channel opening.[4] The diversity of nAChR subtypes and their putative, distinctive roles in different functions provides an opportunity, in principle, to produce subtype-specific ligands that may serve to treat a variety of conditions. However, to date, the high sequence homology across individual subtypes provides a substantial challenge for the development of subtype-selective nicotinic drugs. Nicotinic ligands lacking sufficient subtype-selectivity may cause adverse side effects. For instance, nicotine (**1**) has well-known and epibatidine (**2**) has potential therapeutic benefits for a number of nervous system disorders (Figure 1). However, the therapeutic potential of these two natural products is compromised by their unacceptable side effects arising from their affinity to almost all subtypes of nAChRs, albeit with different potencies. Furthermore, although varenicline (**3**) has been launched and marketed as an α4β2-nAChR partial agonist for the indication of tobacco addiction, peripheral and central side effects, such as nausea, gastrointestinal symptoms, and changes in mood have been observed in some patients.[4, 5] Compound **3** also functions as a full agonist at α7- and α3β4*-nAChRs (the asterisk denotes the possible integration of other subunits into the pentamer), and also as a 5-HT_3 agonist.[6]

Thus, understanding the detailed atomic structure remains crucial to the design of novel nicotinic agents with minimum side effects that selectively target designated receptor subtypes and thus the related nervous-system pathologies to which they are linked. High-resolution crystal structures of integral membrane protein, mammalian nAChRs are not yet available. Nevertheless, the invertebrate pentameric acetylcholine binding proteins (AChBPs), which are structural and functional surrogates for the N-terminal, extracellular ligand-binding domain (LBD) of nAChRs, are more readily crystallized, and they provide well-studied structural models that provide insights into ligand recognition sites and other elements of nAChR ECDs.[7, 8] To date, AChBPs from several different snail species have been identified, and more than fifty different ligand-bound co-crystal structures have been determined,

facilitating both mechanistic studies and nicotinic drug development. The majority of these structures have been obtained with AChBP from *Aplysia californica* (Ac) or *Lymnaea stagnalis* (Ls), which exhibit substantial differences in affinities for nicotinic ligands and thereby mimic distinct subtypes of nAChR.[9, 10] Recently, a novel AChBP has been identified from the marine annelid *Capitella teleta* (Ct), which more closely mimics α4β2-nAChRs and their high affinity binding of several ligands, including compound **3**, thus providing a potentially useful model to study structural determinants of ligand recognition at this receptor subtype.[11, 12]

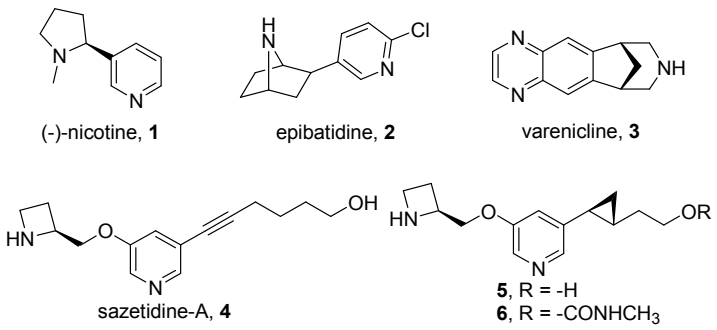

Figure 1. Selected examples of nAChR ligands.

Accumulating evidence suggests that drugs targeting α4β2*-nAChRs, which are the predominant subtype of neuronal nAChRs, may prove useful in the management of major depression.[13, 14] In pursuit of antidepressants that exhibit fewer side effects and act pharmacologically in novel ways, we recently reported the introduction of a chiral cyclopropane ring in place of the acetylene bond in sazetidine-A (**4**) that furnished a series of cyclopropane-containing ligands selective for α4β2-nAChRs.[15, 16] Their superior subtype selectivity makes these compounds stand out among all of the other α4β2-nAChR agonists reported to date, including the marketed drug **3**. One of the most promising compounds, **5**, displays sub-nanomolar binding affinity at α4β2-nAChRs and excellent subtype selectivity over α3β4*- and α7-nAChRs, while acting as a potent α4β2-nAChR partial agonist. Its favorable antidepressant-like effect was demonstrated in the mouse forced swim test, suggesting that compound **5** represents a promising lead for the treatment of depression, and a good progenitor to other potential candidates to advance through the drug discovery pipeline. To provide insight into the structural determinants of compound **5** that confer its remarkable nAChR subtype selectivity, partial agonism, and antidepressant-

like properties, both structural studies and the comprehensive pharmacological analysis of compound **5** were carried out.

Results and Discussion

First, we determined binding affinities (K_i) of selected cyclopropane ligands for Ac- and Ct-AChBP using [^{3}H]epibatidine binding competition assays to evaluate the validity of using these proteins as models for high affinity binding at α4β2-nAChRs. These binding data (Table 1) reveal high affinities of the two cyclopropane ligands for the Ct-AChBP, which are approximately 80-fold higher than those for the Ac-AChBP. Moreover, the K_i values of compound **5** are about 2-fold lower than those of compound **6** for both Ac- and Ct-AChBP, which is in agreement with the previously observed binding data[16] for these two compounds at heterologously expressed α4β2-nAChRs or rat forebrain α4β2*-nAChRs. Taken together, these data demonstrate that compounds **5** and **6** bind with higher affinity to Ct-AChBP than to Ac-AChBP, indicating that Ct-AChBP is more suitable for structural studies of ligand recognition using X-ray crystallography.

Table 1. Ligand dissociation constants (K_i, nM) for Ac- and Ct-AChBP[a]

Ligand	Ac-AChBP	Ct-AChBP	α4β2	α4β2*
5	979±364	12.8±0.4	0.1	0.5
6	1927±458	22±3	0.6	1.7
1	598±108	496±30	4.9	9.8

[a] Experimental procedures see Supporting Information. The binding data for compounds **1**, **5**, and **6** at α4β2- and α4β2*-nAChRs were obtained from reference 16. α4β2*-nAChRs were prepared from rat forebrain.

The X-ray crystal structure of Ct-AChBP in complex with compound **5** (Figure 2) was determined at a resolution of 2.3 Å (Table S1). Figure 2a shows a cartoon representation of Ct-AChBP along the five-fold symmetry axis with the C-terminus of the protein pointing toward the viewer. Difference electron density in all five ligand binding sites of the pentamer unambiguously revealed the occupancy of compound **5** (shown in sphere representation in Figure 2a). Figure 2b shows a magnified stereo view of compound **5** as well as two interacting water molecules (w1 and w2) built into $2F_o–F_c$ electron density

(grey mesh, contoured at 1.2σ). Similar to other nicotinic ligands, compound **5** is bound at the interface between two subunits where it forms interactions with amino acids of loops A, B, and C on the principal subunit and loops D, E, and F on the complementary subunit (in Figure 2c principal and complementary subunits are shown in white and blue, respectively). The azetidinyl moiety of the compound (shown in yellow) protrudes deep inside the binding pocket, whereas the hydroxyethyl group attached to the cyclopropane ring points outward. The nitrogen atom of the azetidinyl moiety forms hydrogen bonds with the carbonyl oxygen of W153 (loop B) and an ordered water molecule (w2), which forms part of a chain of water molecules (w2–w5) extending into the core of the β-sandwich. In addition, the azetidinyl nitrogen forms cation-π interactions with W153 (loop B) and Y201 (loop C). Hydrophobic interactions are formed with the side chains of V154 (loop B) and Y194, Y201 (loop C) and the vicinal disulfide bond between C196 and C197 (loop C). The nitrogen atom of the pyridine ring is involved in a hydrogen bond with a water molecule (w1), which forms a bridge to interact with the peptide backbone atoms of Q116 and I128 (loop E) on the complementary face of the binding pocket. Hydrophobic interactions are formed with the side chains of I118 and F128 (loop E). These interactions are remarkably similar to those observed in the structure of Ct-AChBP in complex with compound **3** (Figure 2d), which also binds with high affinity to Ct-AChBP and acts as a partial agonist at the α4β2-nAChRs.[12] In the compound **3**-bound structure, the ligand interactions also include water molecules that occupy nearly identical positions and bridge interactions within the complementary (w1) and principal (w2–w5) binding sites (Figure 2d). In addition, compound **3** and compound **5** stabilize loop C in similarly identical conformation, which is intermediate between the contracted and extended conformation observed with most agonists and antagonists, respectively.[17] A notable difference between the two structures is the different side chain orientation of F102 (loop A), namely a *g*- versus *t*-rotamer in the compound **5**- and compound **3**-bound structures, respectively. Such rotamer differences of the loop A aromatic residue have also been observed in crystal structures of Ac-AChBP (Y91) and Ls-AChBP (Y89).[18] Remarkably, a superposition of the compound **3**- and compound **5**-bound structures (Figure 2e) demonstrates that both ligands adopt overlapping binding poses and that the two nitrogen

atoms involved in water molecule interactions (w1 and w2, respectively) are in nearly identical locations. This result indicates that compounds with distinct chemical structures can engage in similar interactions, which critically rely on the presence of two cationic centers spaced at ~5.8Å from each other (cationic centers are indicated with arrows in Figure 2e). Together, the results from our Ct-AChBP crystal structures reveal a common mode of interaction for compound **5** and compound **3**, which both act as partial agonists at α4β2-nAChRs.

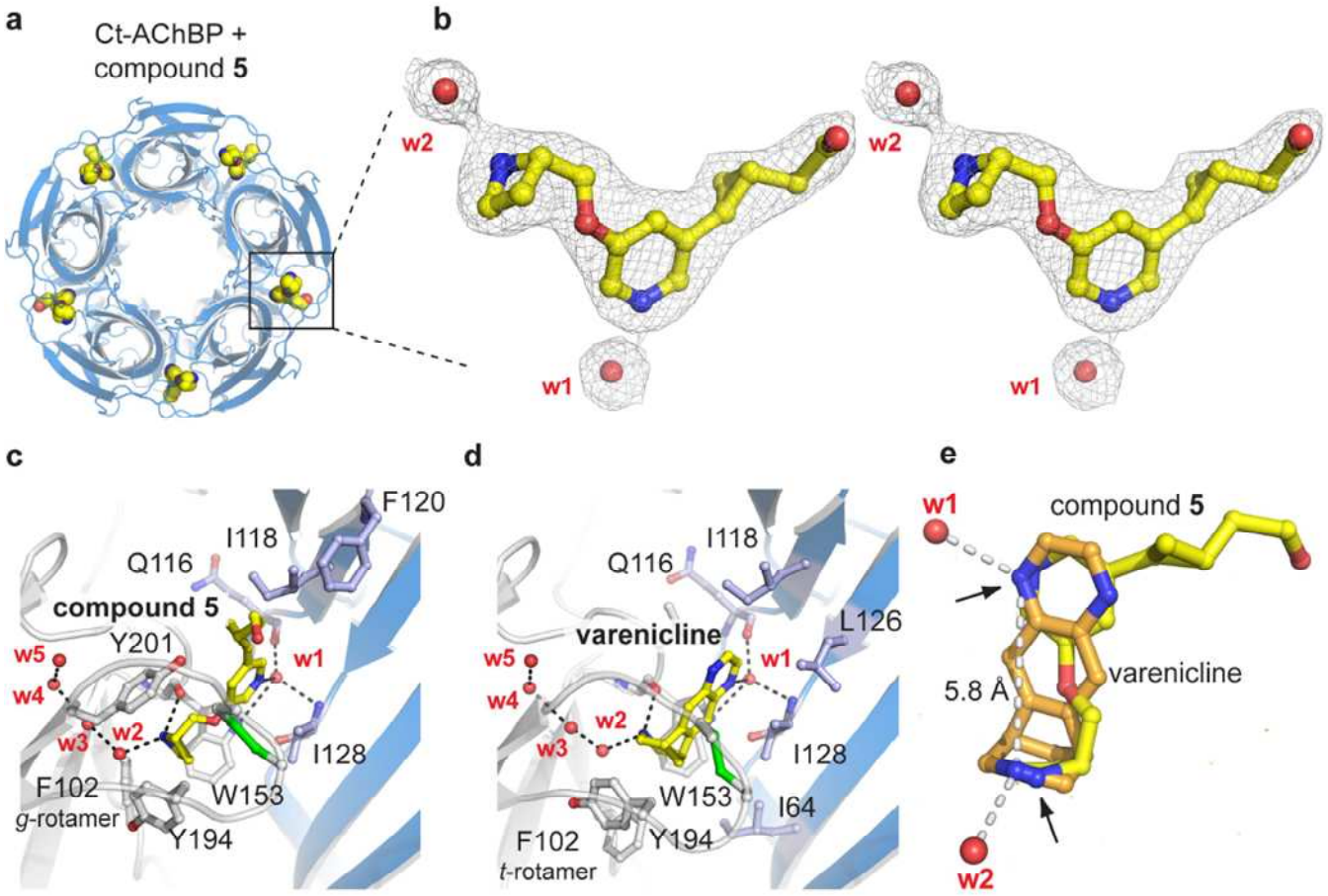

Figure 2. X-ray crystal structure of the Ct-AChBP in complex with compound **5** or compound **3**. (a) Crystal structure of Ct-AChBP in complex with compound **5** as observed along the five-fold symmetry axis. (b) Stereographic view of compound **5** based on its $2F_o$-F_c electron density contour at a 1.2σ level. Carbon = yellow, oxygen = red, nitrogen = blue, sulfur = green in all figures. (c) Ct-AChBP amino acid interactions with compound **5**. (d) Ct-AChBP amino acid interactions with compound **3**. (e) A superposition of bound compound **3** (orange) and compound **5** (yellow).

With the resolved Ct-AChBP structure in hand, and given the greater similarity between human receptor and Ct-AChBP binding data, a computational study was undertaken to generate a Ct-AChBP based homology model for the ligand binding domain of the human α4β2-nAChR. The use of the Ct-AChBP structure as the template is also justified by its high homology with the human α4β2 receptor (as computed by ClustalX: α4/Ct-AChBP = 64.6% and β2/Ct-AChBP = 62.1%) as well as by the acceptable conservation of the key residues involved in ligand recognition (Figure S1). Figure 3 reveals a ribbon structure for the ECD of the modeled, human α4β2 dimer (Figure 3A), which superimposes well on the structure of the Ct-AChBP (Figure 3B). Each monomer shows the typical, ten-stranded β-sandwich capped by an N-terminal α-helix. The two modeled β-sandwich cores can be nicely superimposed on that of Ct-AChBP, whereas some divergence is observed in the superimposition of their peripheral loops, likely due to differences between their sequences and lengths.

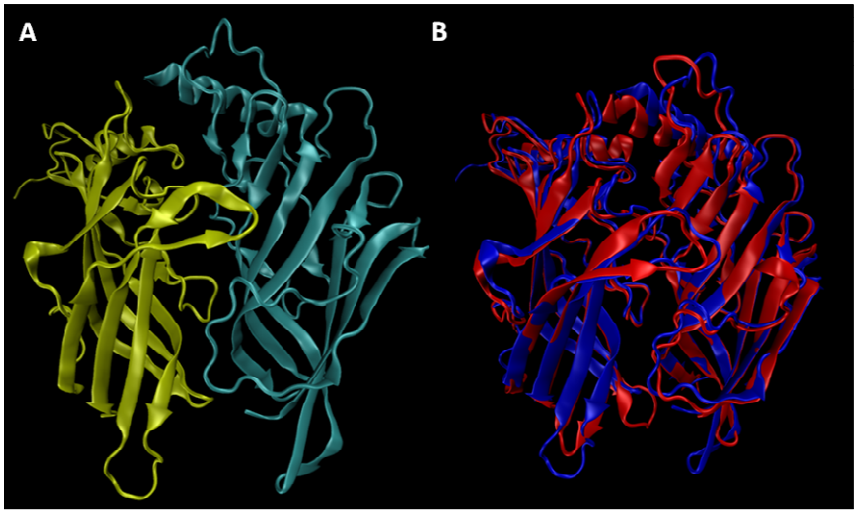

Figure 3. Homology model of the human α4β2-nAChR extracellular domain (ECD) including the ligand binding interface. (3A) Ribbon structure representation colored by subunit (yellow = α4, azure = β2) for the human α4β2-nAChR ECD. (3B) Superimposition of the modeled structure (in blue) with the experimental template from the Ct-AChBP (in red).

The α4β2-nAChR ligand binding site is located at the dimer interface and is lined by residues from loops A–C from the α4 subunit and loops D–E from the β2 subunit, including Y98 (loop A), W154

(loop B), Y195 and Y202 (loop C) as well as W57 (loop D), V111 and L121 (loop E). As depicted in Figure S1, the key residues are well conserved in the Ct-AChBP apart from W57, which is replaced by I64 in the Ct-AChBP, and this induces a deeper arrangement of the W153 side chain in the Ct-AChBP structure compared to that of the homologue W154 residue due to reduced steric hindrance of I64 compared to W57. As documented by Figure S2, the key residues involved in ligand recognition show similar spatial arrangements between Ct-AChBP and human α4β2-nAChR, thus suggesting a generally conserved architecture of the binding sites which reflects on superimposable poses of the docked and resolved compound **5** (see below).

The reliability of the generated model and its interaction properties were then analyzed by docking a set of reported compound **4** derivatives (as compiled in Table S2), including compound **5**, which was co-crystallized with the Ct-AChBP. The best complex obtained for compound **5** within the binding cavity of the human α4β2 model is in encouraging agreement with the X-ray structure (Figure 4A and Figure S2). Indeed, the azetidine ring protrudes deep inside the binding pocket, where it can stabilize pivotal H-bonds with the backbone carbonyl group of S153 and W154 (loop B). The main difference between the computed complex and the resolved one concerns F102 of the Ct-AChBP, which is replaced by Y98 (loop A) in the α4β2-nAChR model, whose hydroxyl group is involved in a clear H-bond with the charged nitrogen atom and may replace the ordered water molecule (w2) as seen in the Ct-AChBP complex. Again, the charged ring stabilizes a set of cation-π interactions (plus various hydrophobic interactions) with the already mentioned Y98 and W153 as well as with W57 (loop D), Y92, (loop A) Y195 and Y202 (loop C). The nitrogen atom of the pyridine ring is involved in an H-bond with the backbone atoms of L121 (loop E), and considering the distance between them (3.3 Å), it might occur both directly and through a bridging water as seen in the Ct-AChBP structure. Finally, the hydroxyethyl group attached to the cyclopropane ring shows an arrangement remarkably similar to that observed in the X-ray complex since it points outward without stabilizing significant polar interactions. In detail, the cyclopropane ring elicits apolar contacts with V111, F119 (loop E) and A199 (loop C),

whereas the hydroxyl group approaches loop C but does not stabilize significant polar interactions apart from a weak H-bond with the backbone atoms of A199. Such a pose confirms that the region at the interface between α4 and β2 subunits can accommodate quite large moieties and this is in agreement with the recent human α4β2 models proposed by Li and co-workers who indeed postulated the existence of a negative allosteric site in this region.[19]

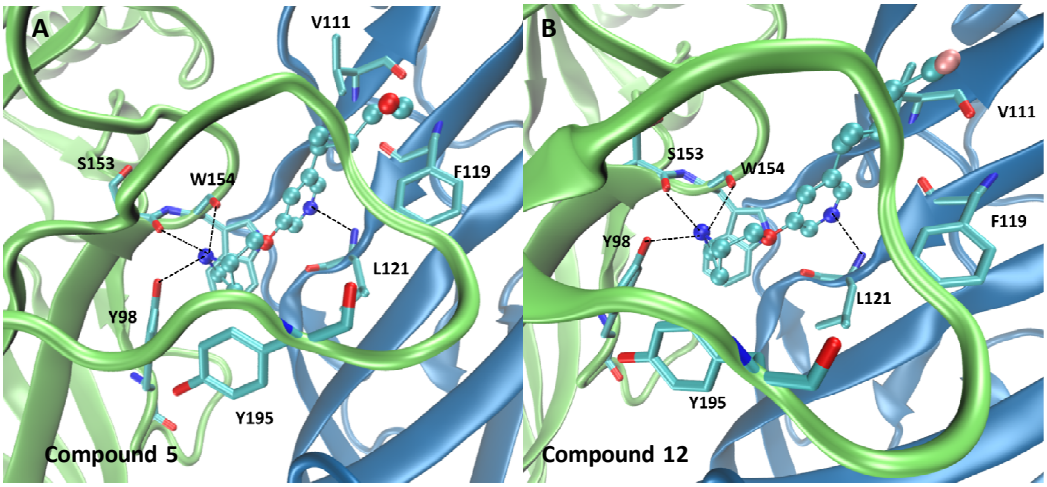

Figure 4. Docking of compounds **5** and **12** at the ligand binding site of the modeled, human α4β2-nAChR extracellular domain. The protein backbone is colored in green for the α4 and in azure for the β2 subunit. Oxygen = red, nitrogen = blue, sulfur = yellow, fluorine = brown in all figures. (4A) Main interactions stabilizing the computed complex between compound **5** and the α4β2-nAChR model. (4B) Main interactions stabilizing the computed complex between compound **12** and the α4β2-nAChR model.

When analyzing the best complexes as generated for the set of docked compound **4** congeners, one may note that most compounds assume a binding mode superimposable to that of compound **5**, since in all monitored complexes, the moieties corresponding to the cyclopropane tail are unable to elicit significant polar interactions with the β2 subunit and remain in the subpocket flanked by loop C. Even the compounds bearing large moieties (as seen for some carbamate derivatives, such as compound **6**) show similar binding modes although these moieties cannot be completely harbored below loop C and

thus partially protrude toward the β2 subunit without stabilizing polar contacts. Indeed, the cyclopropane tail remains in a region around loop C that, as evidenced by Figure S3 for the human model, is surrounded by apolar residues only without contacting polar residues of both α4 and β2 subunits. This suggests that the hydroxyethyl group attached to the cyclopropane ring can be modified by more hydrophobic moieties without producing steric hindrance.

Rational Design and Synthesis of Fluorine-Containing Cyclopropane nAChR Ligands

Based upon our analysis of the Ct-AChBP–compound **5** co-crystal structure together with the molecular docking studies, it is apparent that no strong hydrogen bonding interactions are observed for the hydroxyl group at the terminus of the right-hand side chain, suggesting that this hydroxyl group does not constitute an essential pharmacophoric element for receptor recognition, and may therefore be further modified using other functional groups. Moreover, the free hydroxyl group in compound **5** represents a possible metabolic liability due to potential for oxidation, glucuronidation, sulfation, and other bioconjugations.[20] Consequently, small and hydrophobic functional groups might be able to replace the polar and hydrophilic hydroxyl group thus yield new cyclopropane ligands with improved drug-like properties. In the field of medicinal chemistry, aside from the introduction or presence of nitrogen atoms in the drug scaffolds, the incorporation of fluorine atoms likely constitutes the second most favored hetero-atom that has been incorporated into biologically active molecules. The unique nature of fluorine, including its small size, high electronegativity, and high energy of bond formation to carbon, imparts a variety of advantages to fluorine-containing drugs. These advantages include properties such as enhanced binding interactions, improved metabolic stability, lack of alkylating activity (in contrast to chlorides or bromides), changes in physicochemical properties, and possibly enhanced subtype-selectivity. It is not surprising that about 20% of all drugs currently on the market contain at least one fluorine atom, with many more to come.[21, 22] The length of the C–F bond (1.41 Å) is similar to that of the C–O bond (1.43 Å), suggesting that these atoms are bioisosteres. In addition, it is well accepted that the C–F unit may participate in electrostatic interactions responsible for strengthening

ligand-protein binding interactions.[23] With these considerations in mind, we designed analogs of compound **5** in which the hydroxyl group is substituted with either hydrogen or fluorine atoms (compounds **10**, **12**, and **13**). As shown in Table S3, the blood-brain barrier (BBB) permeability of these new analogs, as estimated by their calculated logBB values, increases from -0.5 to about -0.1, which is similar to the logBB of compound **3**. Drug permeability across the BBB is, of course, essential to obtaining therapeutic drug levels in the brain, as this is where the targeted α4β2-nAChRs are expressed.[24] These numbers suggest a beneficial effect of the replacement of the hydroxyl group with either hydrogen or fluorine atoms on BBB penetration and subsequent bioavailability.

Docking simulations of the three proposed compounds confirm the reliability of such modifications since all derivatives assume poses almost superimposable to that of compound **5** and stabilize reinforced hydrophobic interactions with the region surrounding loop C. Thus, Figure 4B illustrates the best complex for compound **12**, showing that it stabilizes the same interaction pattern already observed for compound **5** involving the azetidine and the pyridine rings. Notably, Figure 4B shows that the fluorine atom is inserted in a markedly hydrophobic niche lined by V111, F119, and the characteristic disulphide bridge of loop C (C197–C198) thus confirming the relevance of the apolar contacts elicited by this moiety.

The synthesis of compounds **10**, **12**, and **13** is described in Scheme 1. For the terminal methyl compound, the optically pure alcohol **7**[16] was acylated with isobutyric anhydride and the benzyl group was removed by hydrogenolysis, followed by installation of the azetidine moiety by a modified Mitsunobu reaction to obtain the intermediate **8**. After removal of the isobutyryl group, the alcohol intermediate was subjected to standard Swern oxidation and Wittig reaction to furnish the olefin **9**. Successive hydrogenation of the terminal double bond and removal of the Boc group smoothly gave the target compound **10** as its trifluoroacetate salt. For the fluorine-containing analogs, the starting alcohol **11**[16] was tosylated followed by reaction with *n*-tetrabutylammonium fluoride. Boc deprotection of the resulting fluoride yielded compound **12** as its trifluoroacetate salt. Similarly, the aldehyde prepared from the same alcohol **11** by Swern oxidation was converted to *gem*-difluoride using the stable and mild

reagent, (diethylamino)difluorosulfonium tetrafluoroborate (XtalFluor-E), in conjunction with Et_3N•3HF as a promoter.[25] After removal of the Boc group, the resulting *gem*-difluoride **13** was obtained as its trifluoroacetate salt.

Scheme 1. Synthesis of compounds **10**, **12**, and **13**[a]

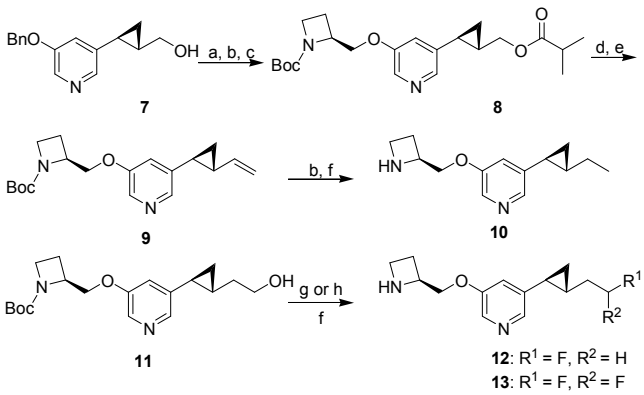

[a] Conditions: (a) isobutyric anhydride, cat. DMAP, Et_3N, CH_2Cl_2, 0 °C to rt; (b) 10% Pd/C, H_2, EtOAc/MeOH, rt; (c) 1-(*tert*-butoxycarbonyl)-(2*S*)-azetidinylmethanol, azodicarbonyldipiperidide (ADDP), P(*n*-Bu)$_3$, PhMe, 0 °C to rt; (d) NaOMe, MeOH, 40 °C; (e) i. $(COCl)_2$, DMSO, Et_3N, CH_2Cl_2, -78 °C; ii. $Ph_3P{=}CH_2$, THF, 0 °C; (f) CF_3COOH, CH_2Cl_2, rt; (g) i. TsCl, Et_3N, CH_2Cl_2, 0 °C to rt; ii. *n*-Bu_4NF, THF, rt; (h) i. $(COCl)_2$, DMSO, Et_3N, CH_2Cl_2, -78 °C; ii. XtalFluor-E, Et_3N•3HF, CH_2Cl_2, rt.

In Vitro Radioligand Binding and Functional Studies.

The K_i values of all of the synthesized cyclopropane compounds, **10**, **12**, and **13** were evaluated by [^{3}H]epibatidine binding competition assays at seven heterologously expressed rat nAChR subtypes. As shown in Table 2, compounds **10**, **12**, and **13** exhibited subnanomolar to low nanomolar binding affinities for both the α4β2- and α4β2*-nAChRs, which are comparable to those of compound **5**. This confirms that the interactions elicited by the cyclopropyl tail are restricted to apolar contacts only and the hydroxyl group does not take part in the binding process. All three of these compounds demonstrated good selectivity for nAChRs containing β2 subunits (α2β2-, α3β2-, α4β2-, and α4β2*-nAChRs) over β4 subunits (α3β4-, α2β4-, and α4β4-nAChRs). As it is known that α3β4*-nAChRs mediate autonomic nicotinic signaling, interaction with these receptors is likely to contribute to adverse side

effects.[1, 26] With the exception of compound **10**, the selectivity for α4β2- over α3β4-nAChRs of compounds **12** and **13** are greater than 16000-fold, suggesting that few if any peripheral side effects should be observed.

Table 2. Binding affinities of cyclopropane ligands and nicotine at seven nAChR subtypes[a]

Compd.	K_i (nM)						
	α2β2	α2β4	α3β2	α3β4	α4β2	α4β2*	α4β4
5	0.1	249	3.0	6520	0.1	0.5	82.6
10	0.4	41.8±9	10.3±1.8	852.1	0.4±0.1	1.2±0.2	14.8±2.8
12	0.4±0.1	137.6	6.1±1.9	3224	0.2	0.9±0.1	39.1±5.6
13	0.3±0.1	85.4±15.1	6.9±1	1976	0.1	0.8±0.2	23±3.1
1	5.5	70	29	260	4.9	9.8	23

[a] Experimental procedures see PDSP Assay Protocol Book (http://pdsp.med.unc.edu/). α4β2*-nAChRs were prepared from rat forebrain. The binding data for compounds **1** and **5** were obtained from reference 16. SEM values are not provided for K_i values > 100 nM.

Next, the functional activity of compounds **10**, **12**, and **13** at the human α4β2-, α3β4*-, and α1β1γδ-nAChRs was determined using the $^{86}Rb^+$ ion flux assays and SH-EP1, SH-SY5Y, and TE671/RD cells, respectively (Table 3, Figure S4).[27-30] All three of these ligands were found to be highly potent, partial agonists at the mixture of high sensitivity (HS) and low sensitivity (LS) α4β2-nAChRs having weak if any agonist activity at α3β4*- or α1β1γδ-nAChRs (Figure S4). Their efficacies ranged from 68–76% of the response to a maximally-efficacious concentration of the full agonist, carbamylcholine, for actions at HS α4β2-nAChRs. At LS α4β2-nAChRs, these ligands had no measurable efficacy as agonists. Their inactivation of nAChR function (following 10 min pre-exposure; blockade of carbamylcholine stimulation) was most potent for α4β2-nAChRs and weak or absent out to 3 μM for actions at α3β4*- or α1β1γδ-nAChRs, respectively. Consistent with the binding data, the fluorine-containing compounds **12** and **13** were about 2-fold more potent than compound **10**, both in agonism and functional inactivation at α4β2-nAChRs, which is similar to that seen for parent compound **5**. The absence or weakness of agonist or antagonist activity at ganglionic α3β4*- or muscle-type α1β1γδ-nAChRs indicates that the occurrence of peripheral side effects is unlikely. When taking all the present data into

account, the presence of a fluorine at the terminus of the side chain appendage leads to a compound with an improved pharmacological profile compared to a hydrogen atom, as not only is high affinity for α4β2-nAChRs maintained, but so is the excellent selectivity over α3β4*-nAChRs.

Table 3. Potencies and efficacies of ligand agonism and inactivation at α4β2-nAChRs[a]

Compd.	Agonism			Inactivation		
	EC_{50} (nM)	Efficacy at HS (%)	Hill slope	IC_{50} (nM)	Efficacy (%)	Hill Slope
5	10.2×/÷1.7	92±6	1.0±0.4	9.4×/÷1.1	62±1	-1.4±0.2
10	19.1×/÷1.2	68±4	1.1±0.2	22.2×/÷1.4	87±4	-1.1±0.3
12	11.3×/÷1.4	76±6	1.3±0.5	10.2×/÷1.3	81±4	-1.2±0.4
13	8.8×/÷1.2	75±7	1.4±0.4	8.6×/÷1.3	86±4	-1.1±0.3
1	290×/÷1.1	88±2*	1.0±0.1	430×/÷1.1	92±2	-0.8±0.09

[a] Experimental procedures see reference16. Potencies (EC_{50} or IC_{50} values) and inactivation efficacies were measured for actions at a mixture of high-sensitivity (HS) and low-sensitivity (LS) α4β2-nAChRs. Due to the semi-logarithmic nonlinear regression analysis, the SEM for EC_{50} or IC_{50} values is not symmetric in linear space. EC_{50} or IC_{50} values are therefore reported with a multiplying/dividing factor. Agonism efficacy values were extrapolated using sazetidine-A defined as a full agonist at the HS α4β2-nAChR (see Supporting Information for details). Results for compounds **1** and **5** were obtained from reference 16. *The efficacy of agonism for compound **1** was available only for a mixed population of HS and LS α4β2-nAChRs. The efficacy of agonism for all other compounds at LS α4β2-nAChRs was approximately zero.

Behavioral Pharmacology and Metabolic Stability Test

To acquire preliminary *in vivo* evaluation of our nicotinic ligands for behavioral effects relevant to psychiatric disease, we used SmartCube®,[31] an automated system in which behaviors of compound-treated mice are captured by digital video and analyzed with computer algorithms. We compared the behavioral signature of a test compound to a database of behavioral signatures obtained using a large set of diverse reference compounds. In this way, the neuropharmacological effects of a test compound can be predicted by similarity to major classes of compounds, such as antipsychotics, anxiolytics, and

antidepressants. As shown in Figure 5, all of the selected nicotinic ligands produced, in most cases, dose-dependent behavioral signatures that are quite different from that of the vehicle, and contained an antidepressant-anxiolytic component and other therapeutic signatures. All of the compounds showed no or a minor profile of side effects.

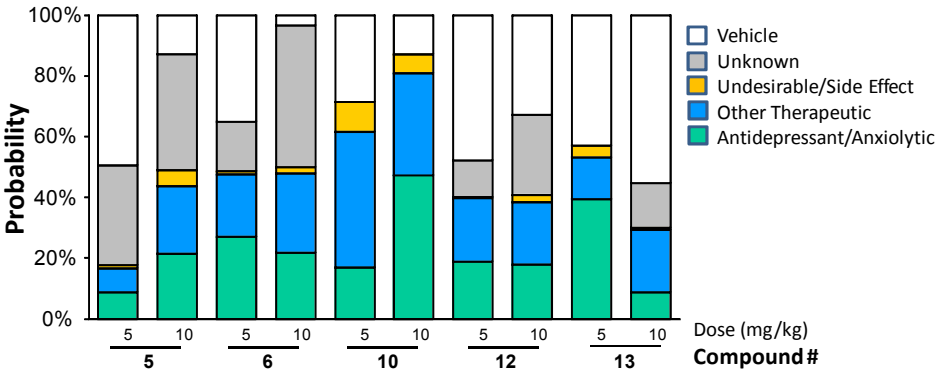

Figure 5. All of the cyclopropane-containing α4β2-nAChRs partial agonists **5**, **6**, **10**, **12**, and **13** produced a signature of activity suggesting potential antidepressant-like effect. The drug was injected i.p., 15 min before testing.

Next, the antidepressant-like properties of compounds **10**, **12**, and **13** were further demonstrated in the classical mouse forced swim test,[32] an assay in which mice are placed into a beaker of water and the time the mouse spends passively floating in the water (immobility) is recorded. Most traditional antidepressants decrease the amount of time the mouse spends immobile. Mice were administered compound, **10**, **12** or **13**, or the selective serotonin reuptake inhibitor, sertraline, as a positive control (20 mg/kg). Compounds **10** and **13**, the least potent and the most potent ligands *in vitro*, had no significant effect in the forced swim test when administered intraperitoneally at doses of 3 or 10 mg/kg. In contrast, compound **12** exhibited an antidepressant-like effect when administered intraperitoneally or orally, with a significant reduction in immobility at the minimal dose of 3 mg/kg (Figure 6).

Additionally, we note that the carbamate derivative **6** reported in our previous publication[16] was metabolically more stable than the hydroxyl compound **5** in the microsomal stability assays (98% vs 80% of the tested compound remained unchanged after 1 h of incubation with a starting concentration of 1 μM). In this context, the fluorinated compound **12** is likely to possess enhanced metabolic stability

compared to the hydroxyl compound **5**, as the hydroxyl group of the latter compound is likely to undergo oxidation and/or bioconjugation reactions.[33] Incubation with mouse, rat, dog, and human liver microsomes[34] demonstrated that no less than 98% of compound **12** remained unchanged after 1 h of incubation at a starting concentration of 2 μM, thereby supporting the greater metabolic stability of the fluorinated compound **12** relative to its parent compound **5**.

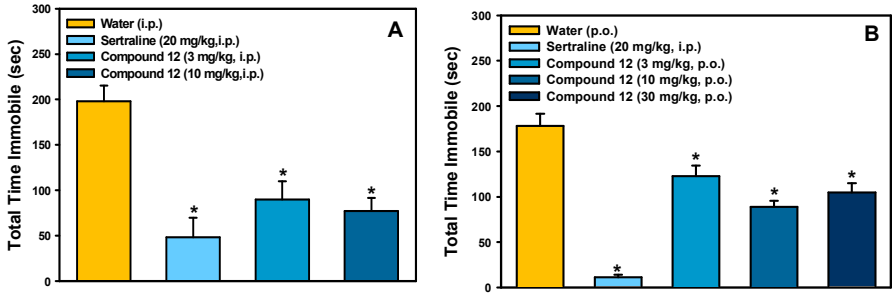

Figure 6. Mouse forced swim data for compound **12**. The selective serotonin reuptake inhibitor, sertraline, produced the expected decrease in immobility. (ANOVAs: F (3,36) = 12.38, $p < 0.001$ (left); F (4,44) = 38.97, $p < 0.001$ (right). *Fisher's PLSD post-hoc test: $ps < 0.05$ vs vehicle). n = 9—10/group.

Conclusions

Herein we have used the X-ray structure of the α4β2-nAChR partial agonist **5** in complex with Ct-AChBP to refine our homology model of the human α4β2-nAChR. By combining homology modeling methods with *in silico* ADME calculations, we in turn designed and synthesized several new analogs of compound **5**. The *in vitro* binding and functional data as well as the *in vivo* behavioral efficacy obtained for the fluorinated compound **12** were found to be comparable to the same parameters obtained for parent hydroxyl containing compound **5**. Additionally, as expected based upon the time-tested principles of medicinal chemistry, the metabolic stability of analog **12** is better than that of **5**. The more limited metabolic stability of **5**, which is subject to both oxidation and bioconjugation reactions, conspires to make this compound a suboptimal drug-like molecule. Of greatest significance is the structural information gleaned from the co-crystal structure of compound **5** in complex with Ct-AChBP. This particular structure has enabled us to refine our homology model of the human α4β2-nAChR, and as

such we anticipate that we will be able to design other chemical scaffolds with which to interrogate these important brain receptors, thus providing the opportunity to create improved therapeutics for a host of pathophysiological mechanisms.

Experimental Section

General Procedures for SmartCube®. Drugs were injected 15 min before the test, during which multiple challenges were presented over the course of the test session. At least 12 mice were used in each treatment group. Digital videos of the subjects were processed with computer vision algorithms to extract over 2000 dependent measures including frequency and duration of behavioral states such as grooming, rearing, etc., and many other features obtained during the test session. These data were compared against a standard database of therapeutic class signatures obtained with the same experimental protocol. The database comprises 14 classes of drugs with some of the major classes, such as the antidepressant class, comprising several subclasses with representatives of most of the drugs in the market. Using machine learning techniques, the reference database was combed to find reference drug class signatures. The best performing techniques were chosen from our evaluation tests and used to build classifiers that capture the therapeutic class signatures. The behavioral signatures of the test compound were then assessed quantitatively with these classifiers to predict total and specific potential therapeutic utility.[31, 35] We present the major signatures in four general groups: antidepressants and anxiolytics, other therapeutics effects, side effects and signatures not recognized by the classifiers, and similarity to vehicle (inactivity).

General Chemistry. All chemicals were purchased from Sigma-Aldrich or Chem-Impex, and solvents were used as obtained from Fisher Scientific or Sigma-Aldrich without further purification. Anhydrous THF and CH_2Cl_2 were obtained by distillation over sodium wire or CaH_2, respectively. All non-aqueous reactions were run under an argon atmosphere with exclusion of moisture from reagents, and all reaction vessels were oven-dried. The progress of reactions was monitored by TLC on SiO_2. Spots were visualized by their quenching of the fluorescence of an indicator admixed to the SiO_2 layer, or by dipping into I_2/SiO_2 mixture. Products were purified by column chromatography on 230–400 mesh SiO_2.

Proton and carbon NMR spectra were recorded at spectrometer frequencies of 400 MHz and 100 MHz, respectively. NMR chemical shifts were reported in δ (ppm) using the δ 7.26 signal of $CHCl_3$ (^{1}H NMR), the δ 4.80 signal of HDO (^{1}H NMR), and the δ 77.23 signal of $CDCl_3$ (^{13}C NMR) as internal standards. ^{13}C NMR spectra in D_2O were not adjusted. Optical rotation was detected on an Autopol IV automatic polarimeter. Mass spectra were measured in the ESI mode at an ionization potential of 70 eV with an LC-MS MSD (Hewlett Packard). The final compounds were purified by preparative HPLC, which was carried out on an ACE 5 AQ column (150 × 20 mm), with detection at 254 and 280 nm on a Shimadzu SPD-10A VP detector; flow rate = 17.0 mL/min; gradient of 0 to 50% methanol in water (both containing 0.05 vol% of CF_3COOH) in 30 min. Purities of final compounds (> 98%) were established by both elemental analysis and by analytical HPLC, which was carried out on an Agilent 1100 HPLC system with a Synergi 4 μm Hydro-RP 80A column, with detection at 254 or 280 nm on a variable wavelength detector G1314A; flow rate = 1.4 mL/min; gradient of 0 to 100% methanol in water (both containing 0.05 vol% of CF_3COOH) in 18 min.

3-[(2(S)-Azetidinyl)methoxy]-5-((1S,2S)-2-ethylcyclopropyl)pyridine Trifluoroacetate (10).

^{1}H NMR (D_2O): δ 8.29 (s, 1H), 8.19 (s, 1H), 7.81 (s, 1H), 4.95 (m, 1H), 4.50 (d, *J* = 4.0 Hz, 2H), 4.17-4.02 (m, 2H), 2.68 (q, *J* = 8.4 Hz, 2H), 1.88 (m, 1H), 1.48-1.35 (m, 2H), 1.25 (m, 1H), 1.08 (m, 2H), 0.95 (t, *J* = 7.2 Hz, 3H); ^{13}C NMR (D_2O): δ 162.6 (TFA), 156.2, 147.3, 132.2, 128.2, 125.4, 116.2 (TFA), 67.5, 58.6, 43.6, 27.6, 26.3, 20.2, 19.9, 17.1, 12.4; $[\alpha]_D^{20}$ = +32.7 (*c* 0.22, MeOH); HPLC purity 99.2%, t_R = 11.9 min; Anal. Calcd for $C_{14}H_{20}N_2O$•2.25CF_3COOH•0.4H_2O: C, 44.79; H, 4.68; F, 25.85; N, 5.65. Found: C, 44.67; H, 4.53; F, 25.79; N, 5.62.

3-[(2(S)-Azetidinyl)methoxy]-5-[(1S,2R)-2-(2-fluoroethyl)cyclopropyl]pyridine Trifluoroacetate (12).

^{1}H NMR (D_2O): δ 8.32 (s, 1H), 8.22 (s, 1H), 7.85 (s, 1H), 4.95 (m, 1H), 4.66 (t, *J* = 6.0 Hz, 1H), 4.55-4.50 (m, 3H), 4.10 (m, 2H), 2.68 (q, *J* = 8.4 Hz, 2H), 1.99 (m, 1H), 1.82 (m, 2H), 1.37 (m, 1H), 1.17 (m, 2H); ^{13}C NMR (D_2O): δ 162.1 (TFA), 155.8, 146.0, 132.0, 128.1, 125.4, 115.8 (TFA), 84.3 (d, $J_{C\text{-}F}$ = 157.7 Hz), 67.1, 58.2, 43.2, 33.2 (d, $J_{C\text{-}F}$ = 18.9 Hz), 21.1, 19.8, 19.2, 15.8; ^{19}F NMR (D_2O): δ -75.7, -

217.8. $[\alpha]_D^{20}$ = +33.8 (*c* 0.26, MeOH); HPLC purity 99.4%, t_R = 6.4 min; Anal. Calcd for $C_{14}H_{19}FN_2O$•2.0CF_3COOH•0.8H_2O: C, 43.87; H, 4.62; F, 26.99; N, 5.68. Found: C, 43.51; H, 4.23; F, 26.80; N, 5.58.

3-[(2(S)-Azetidinyl)methoxy]-5-[(1S,2R)-2-(2,2-difluoroethyl)cyclopropyl]pyridine Trifluoroacetate (13).

^{1}H NMR (D_2O): δ 8.34 (s, 1H), 8.25 (s, 1H), 7.87 (s, 1H), 6.04 (tt, J_{H-F} = 56.4 Hz, J_{H-H} = 4.0 Hz, 1H), 4.97 (m, 1H), 4.51 (d, *J* = 4.0 Hz, 2H), 4.10 (m, 2H), 2.68 (t, J_{H-F} = 8.4 Hz, 2H), 2.09-1.92 (m, 3H), 1.38 (m, 1H), 1.22 (m, 2H); ^{13}C NMR (D_2O): δ 162.2 (TFA), 155.9, 145.3, 132.2, 128.3, 125.7, 117.1 (t, J_{C-F} = 235.9 Hz), 115.8 (TFA), 67.1, 58.2, 43.2, 36.5 (t, J_{C-F} = 20.9 Hz), 19.8, 19.0, 17.2 (t, J_{C-F} = 7.4 Hz), 15.0; ^{19}F NMR (D_2O): δ -75.8, -116.5. $[\alpha]_D^{20}$ = +25.0 (*c* 0.2, MeOH); HPLC purity 99.3%, t_R = 6.3 min; Anal. Calcd for $C_{14}H_{18}F_2N_2O$•2.7CF_3COOH•1.2H_2O: C, 38.98; H, 3.89; F, 32.10; N, 4.69. Found: C, 38.91; H, 3.58; F, 31.81; N, 4.65.

ASSOCIATED CONTENT

Supporting Information

Synthetic procedures and compound characterizations, crystallization and data collection, computational methods, and behavioral studies. This material is available free of charge via the Internet at http://pubs.acs.org.

Accession Codes

PDB code: 4B5D for the X-ray crystal structure of Ct-AChBP in complex with compound **5**.

AUTHOR INFORMATION

Corresponding Author

*To whom correspondence should be addressed. E-mail: Ronald.Lukas@DignityHealth.org [pharmacology], dani.brunner@psychogenics.com [rodent behavior], giulio.vistoli@unimi.it [modeling], chris.ulens@med.kuleuven.be [X-ray], and kozikowa@uic.edu [medicinal chemistry].

ACKNOWLEDGMENTS. This research was supported by award No. U19MH085193 from the National Institute of Mental Health. We thank the PDSP program for assistance through providing the binding affinity data. CU, ABS, and RvE have received funding from the European Union Seventh Framework Programme under grant agreement n° HEALTH-F2-2007-202088 ("NeuroCypres" project).

ABBREVIATIONS USED

nAChR(s), nicotinic acetylcholine receptor(s); LGICs, ligand-gated ion channels; ECD, extracellular domain; ACh, acetylcholine; AChBP(s), acetylcholine binding protein(s), LBD, ligand-binding domain; Ac, *Aplysia californica*; Ls, *Lymnaea stagnalis*; Ct, *Capitella teleta*; BBB, blood-brain barrier; XtalFluor-E, (diethylamino)difluorosulfonium tetrafluoroborate; HS, high sensitivity; LS, low sensitivity; TFA, trifluoroacetic acid.

REFERENCES

1. Gotti, C.; Clementi, F.; Fornari, A.; Gaimarri, A.; Guiducci, S.; Manfredi, I.; Moretti, M.; Pedrazzi, P.; Pucci, L.; Zoli, M. Structural and functional diversity of native brain neuronal nicotinic receptors. *Biochem. Pharmacol.* **2009**, *78*, 703-711.

2. Jensen, A. A.; Frolund, B.; Liljefors, T.; Krogsgaard-Larsen, P. Neuronal nicotinic acetylcholine receptors: structural revelations, target identifications, and therapeutic inspirations. *J. Med. Chem.* **2005**, *48*, 4705-4745.

3. D'Hoedt, D.; Bertrand, D. Nicotinic acetylcholine receptors: an overview on drug discovery. *Expert Opin. Ther. Targets* **2009**, *13*, 395-411.

4. Taly, A.; Corringer, P. J.; Guedin, D.; Lestage, P.; Changeux, J. P. Nicotinic receptors: allosteric transitions and therapeutic targets in the nervous system. *Nat. Rev. Drug Discovery* **2009**, *8*, 733-750.

5. Leung, L. K.; Patafio, F. M.; Rosser, W. W. Gastrointestinal adverse effects of varenicline at maintenance dose: a meta-analysis. *BMC Clin. Pharmacol.* **2011**, *11*, 15-22.

6. Lummis, S. C.; Thompson, A. J.; Bencherif, M.; Lester, H. A. Varenicline is a potent agonist of the human 5-hydroxytryptamine3 receptor. *J. Pharmacol. Exp. Ther.* **2011**, *339*, 125-131.

7. Brejc, K.; van Dijk, W. J.; Klaassen, R. V.; Schuurmans, M.; van Der Oost, J.; Smit, A. B.; Sixma, T. K. Crystal structure of an ACh-binding protein reveals the ligand-binding domain of nicotinic receptors. *Nature* **2001**, *411*, 269-276.

8. Rucktooa, P.; Smit, A. B.; Sixma, T. K. Insight in nAChR subtype selectivity from AChBP crystal structures. *Biochem. Pharmacol.* **2009**, *78*, 777-787.

9. Celie, P. H.; van Rossum-Fikkert, S. E.; van Dijk, W. J.; Brejc, K.; Smit, A. B.; Sixma, T. K. Nicotine and carbamylcholine binding to nicotinic acetylcholine receptors as studied in AChBP crystal structures. *Neuron* **2004**, *41*, 907-914.

10. Hansen, S. B.; Talley, T. T.; Radic, Z.; Taylor, P. Structural and ligand recognition characteristics of an acetylcholine-binding protein from Aplysia californica. *J. Biol. Chem.* **2004**, *279*, 24197-24202.

11. McCormack, T.; Petrovich, R. M.; Mercier, K. A.; DeRose, E. F.; Cuneo, M. J.; Williams, J.; Johnson, K. L.; Lamb, P. W.; London, R. E.; Yakel, J. L. Identification and functional characterization of a novel acetylcholine-binding protein from the marine annelid Capitella teleta. *Biochemistry* **2010**, *49*, 2279-2287.

12. Billen, B.; Spurny, R.; Brams, M.; van Elk, R.; Valera-Kummer, S.; Yakel, J. L.; Voets, T.; Bertrand, D.; Smit, A. B.; Ulens, C. Molecular actions of smoking cessation drugs at alpha4beta2 nicotinic receptors defined in crystal structures of a homologous binding protein. *Proc. Natl. Acad. Sci. U.S.A.* **2012**, *109*, 9173-9178.

13. Philip, N. S.; Carpenter, L. L.; Tyrka, A. R.; Price, L. H. Nicotinic acetylcholine receptors and depression: a review of the preclinical and clinical literature. *Psychopharmacology (Berl)* **2010**, *212*, 1-12.

14. Mineur, Y. S.; Picciotto, M. R. Nicotine receptors and depression: revisiting and revising the cholinergic hypothesis. *Trends Pharmacol. Sci.* **2010**, *31*, 580-586.

15. Kozikowski, A. P.; Eaton, J. B.; Bajjuri, K. M.; Chellappan, S. K.; Chen, Y.; Karadi, S.; He, R.; Caldarone, B.; Manzano, M.; Yuen, P. W.; Lukas, R. J. Chemistry and pharmacology of nicotinic

ligands based on 6-[5-(azetidin-2-ylmethoxy)pyridin-3-yl]hex-5-yn-1-ol (AMOP-H-OH) for possible use in depression. *ChemMedChem* **2009**, *4*, 1279-1291.

16. Zhang, H.; Tückmantel, W.; Eaton, J. B.; Yuen, P. W.; Yu, L. F.; Bajjuri, K. M.; Fedolak, A.; Wang, D.; Ghavami, A.; Caldarone, B.; Paterson, N. E.; Lowe, D. A.; Brunner, D.; Lukas, R. J.; Kozikowski, A. P. Chemistry and behavioral studies identify chiral cyclopropanes as selective alpha4beta2-nicotinic acetylcholine receptor partial agonists exhibiting an antidepressant profile. *J. Med. Chem.* **2012**, *55*, 717-724.

17. Brams, M.; Pandya, A.; Kuzmin, D.; van Elk, R.; Krijnen, L.; Yakel, J. L.; Tsetlin, V.; Smit, A. B.; Ulens, C. A structural and mutagenic blueprint for molecular recognition of strychnine and d-tubocurarine by different cys-loop receptors. *PLoS. Biol.* **2011**, *9*, e1001034.

18. Edink, E.; Rucktooa, P.; Retra, K.; Akdemir, A.; Nahar, T.; Zuiderveld, O.; van Elk, R.; Janssen, E.; van Nierop, P.; van Muijlwijk-Koezen, J.; Smit, A. B.; Sixma, T. K.; Leurs, R.; de Esch, I. J. Fragment growing induces conformational changes in acetylcholine-binding protein: a structural and thermodynamic analysis. *J. Am. Chem. Soc.* **2011**, *133*, 5363-5371.

19. Henderson, B. J.; Pavlovicz, R. E.; Allen, J. D.; Gonzalez-Cestari, T. F.; Orac, C. M.; Bonnell, A. B.; Zhu, M. X.; Boyd, R. T.; Li, C.; Bergmeier, S. C.; McKay, D. B. Negative allosteric modulators that target human alpha4beta2 neuronal nicotinic receptors. *J. Pharmacol. Exp. Ther.* **2010**, *334*, 761-774.

20. Shu, Y. Z.; Johnson, B. M.; Yang, T. J. Role of biotransformation studies in minimizing metabolism-related liabilities in drug discovery. *AAPS J.* **2008**, *10*, 178-192.

21. O'Hagan, D. Understanding organofluorine chemistry. An introduction to the C-F bond. *Chem. Soc. Rev.* **2008**, *37*, 308-319.

22. Purser, S.; Moore, P. R.; Swallow, S.; Gouverneur, V. Fluorine in medicinal chemistry. *Chem. Soc. Rev.* **2008**, *37*, 320-330.

23. Muller, K.; Faeh, C.; Diederich, F. Fluorine in pharmaceuticals: looking beyond intuition. *Science* **2007**, *317*, 1881-1886.

24. Alavijeh, M. S.; Chishty, M.; Qaiser, M. Z.; Palmer, A. M. Drug metabolism and pharmacokinetics, the blood-brain barrier, and central nervous system drug discovery. *NeuroRx* **2005**, *2*, 554-571.

25. L'Heureux, A.; Beaulieu, F.; Bennett, C.; Bill, D. R.; Clayton, S.; Laflamme, F.; Mirmehrabi, M.; Tadayon, S.; Tovell, D.; Couturier, M. Aminodifluorosulfinium salts: selective fluorination reagents with enhanced thermal stability and ease of handling. *J. Org. Chem.* **2010**, *75*, 3401-3411.

26. Sullivan, J. P.; Bannon, A. W. Epibatidine: Pharmacological Properties of a Novel Nicotinic Acetylcholine Receptor Agonist and Analgesic Agent. *CNS Drug Reviews* **1996**, *2*, 21-39.

27. Lukas, R. J.; Norman, S. A.; Lucero, L. Characterization of Nicotinic Acetylcholine Receptors Expressed by Cells of the SH-SY5Y Human Neuroblastoma Clonal Line. *Mol. Cell Neurosci.* **1993**, *4*, 1-12.

28. Lukas, R. J. Cell lines as models for studies of nicotinic acetylcholine receptors. In *Neuronal Nicotinic Receptors: Pharmacology and Therapeutic Opportunities*; Wiley-Liss, Inc, New York: **1999**; pp 81-97.

29. Lukas, R. J.; Fryer, J. D.; Eaton, J. B.; Gentry, C. L. Some methods for studies of nicotinic acetylcholine receptor pharmacology. In *Nicotinic Receptors and the Nervous System*; CRC Press, Boca Raton: **2002**; pp 3-27.

30. Eaton, J. B.; Peng, J. H.; Schroeder, K. M.; George, A. A.; Fryer, J. D.; Krishnan, C.; Buhlman, L.; Kuo, Y. P.; Steinlein, O.; Lukas, R. J. Characterization of human alpha4beta2-nicotinic acetylcholine receptors stably and heterologously expressed in native nicotinic receptor-null SH-EP1 human epithelial cells. *Mol. Pharmacol.* **2003**, *64*, 1283-1294.

31. Roberds, S. L.; Filippov, I.; Alexandrov, V.; Hanania, T.; Brunner, D. Rapid, computer vision-enabled murine screening system identifies neuropharmacological potential of two new mechanisms. *Front. Neurosci.* **2011**, *5*, 103.

32. Porsolt, R. D.; Bertin, A.; Jalfre, M. Behavioral despair in mice: a primary screening test for antidepressants. *Arch. Int. Pharmacodyn. Ther.* **1977**, *229*, 327-336.

33. Walsh, J. S.; Miwa, G. T. Bioactivation of drugs: risk and drug design. *Annu. Rev. Pharmacol. Toxicol.* **2011**, *51*, 145-167.

34. The metabolic stability studies were carried out by Cerep, Inc.

35. Houghten, R. A.; Pinilla, C.; Giulianotti, M. A.; Appel, J. R.; Dooley, C. T.; Nefzi, A.; Ostresh, J. M.; Yu, Y.; Maggiora, G. M.; Medina-Franco, J. L.; Brunner, D.; Schneider, J. Strategies for the use of mixture-based synthetic combinatorial libraries: scaffold ranking, direct testing in vivo, and enhanced deconvolution by computational methods. *J. Comb. Chem.* **2008**, *10*, 3-19.

TOC Graphic: